

Metastability induced by non-reciprocal adaptive couplings in Kuramoto models

Sayantan Nag Chowdhury¹ and Hildegard Meyer-Ortmanns^{1,2}

¹*School of Science, Constructor University, P.O.Box 750561, 28725 Bremen, Germany*

²*Complexity Science Hub, Vienna, Austria**

(Dated: December 24, 2025)

Non-reciprocal couplings are frequently found in systems out-of-equilibrium such as neuronal networks. We consider generalized Kuramoto models with non-reciprocal adaptive couplings. The non-reciprocity refers to the type of couplings according to Hebbian or anti-Hebbian rules and to different time scales, on which the couplings evolve. The main effect of this specific combination of deterministic dynamics is an induced metastability of anti-phase synchronized clusters of oscillators. Metastable switching is typical for neuronal networks and a characteristic of brain dynamics. We analyze the metastability as a function of the system parameters, in particular of the size and the network connectivity. The mechanism behind sudden changes in the order parameters are individual oscillators which change their cluster affiliation from time to time, providing “weak ties” between clusters of synchronized oscillators. The time series have random features, but derive from deterministic dynamics.

I. INTRODUCTION

Among complex networks, adaptive networks have attracted much attention over the last years. Adaptation and learning are essential processes in evolution. In chemical networks, the reaction rates may dynamically be adapted to improve the productivity. In social systems, agents may adapt their strategies to those of their friends or imitate the strategies of successful agents. In technical applications, adaptive couplings are used to prevent system’s failures. In relation to neuronal networks, one of the first studies of plasticity and learning in a network of coupled phase oscillators is the work of [1] and somewhat later the work of [2]. More recently, the role of plasticity and adaptation is discussed in a review of [3]. Modular structure on meso- and macroscales can emerge when adaptively reinforced synchronization competes with a constraint on nodes to establish connections with other units of the network [4]. Adaptation is also considered for adaptive multiplex networks, see, for example, the work of [5–7]. Adaptive coupling can have the interesting effect of inducing collective excitability and self-sustained bursting oscillations in globally coupled populations of non-excitatory units [8]. Insights from neural networks with adaptive couplings can be exploited to explain dynamical properties of multi-frequency clusters in power grid networks, described by Kuramoto-Sakaguchi phase oscillators with inertia [9]. The fundamental relation between power grid and neural networks is established in [10]; according to this relation phase oscillator models with inertia correspond to a particular class of adaptive networks. In this paper we will consider special cases of the work of [11–13]. According to the work of [11], a multilayer structure and chimera states emerge in a self-organized way if generalized globally coupled Kuramoto models are con-

sidered with adaptive coupling. Subnetworks of densely coupled elements form sequentially whose size is hierarchically ordered and which decouple as result of the hierarchical structure. If the global coupling in such networks is replaced by a random sparse structure of connections, chimera states form which retain features of a hierarchical organization, and the set of elements that form coherent groups can be rearranged during the network evolution [12]. When the couplings adapt and have their own dynamics, it amounts to plasticity in relation to neuronal networks. In particular, the couplings may change as a function of the timing between the oscillators. If spike-time dependent plasticity enters also the natural frequencies of the oscillators, heterogeneous layered clusters with different frequencies show up from homogeneous oscillator populations [13]. For oscillatory neuronal populations with spike-timing dependent plasticity it is shown in [14] that for an optimal noise level the amount of synaptic coupling gets maximal, leading to noise-induced self-organized synaptic connectivity. Here, the application of noise counteracts desynchronization that would naively be expected as result of noise.

At another frontier, non-reciprocity is topical in systems out-of-equilibrium, since the validity of Newton’s third law (for every action is an equal and opposite reaction) is the exception rather than the rule in these systems. Arguably the most plausible example is from social systems where a relation of friendship holds in one direction but more enmity than friendship in the opposite direction. Populations with conformist and contrarian members are considered in [15]. Non-reciprocity is also found in active matter [16–18], metamaterials [19, 20], or in relation to game theory [21]. Occasionally it is discussed in neuronal networks [1, 22]. In [1] asymmetric networks are considered, where only part of the synaptic connections between pairs of neurons are non-reciprocal and have slow dynamic response with the effect that temporal association becomes possible as recall of time sequences and cycles of patterns. The work of [22] introduces two populations of excitatory and inhibitory populations in

* hmeyerortm@constructor.university

a Kuramoto model with the non-reciprocal feature that each oscillator of the excitatory (inhibitory) population exerts a positive (negative) influence on each oscillator of the inhibitory (excitatory) population, respectively. This way, the Kuramoto model accounts for the onset of excitatory/inhibitory-based neuronal rhythms.

Non-reciprocity can have strong implications on the collective behavior of many-body systems. It may lead to time-dependent phases in which spontaneously broken continuous symmetries are dynamically restored [23]. In view of general manifestations of non-reciprocity, we consider systems with self-organizing structures, of which synchronization is a prototypical form. More specifically, this paper is on non-reciprocity in adaptive networks and its impact on synchronization patterns. The dynamics of nonreciprocal adaptation may be realized in many ways, via the type of favored interaction (alignment or anti-alignment, Hebbian or anti-Hebbian rules), via the choice of time scales, via feedback as in [1] or frequency adaptation to name some of them.

In this paper we focus on generalized Kuramoto models with both non-reciprocal and adaptive couplings. When we combine Hebbian and anti-Hebbian adaptation rules for the couplings, acting on quite different time scales, we observe switching dynamics between metastable states, characterized by anti-phase cluster synchronization (exceptionally also full synchronization) unless the choice of parameters leads to incoherent oscillations.

Many experimental hints exist that typical states in the brain are metastable [24]. The structure of these metastable states is reflected in functional neuroimage experiments. In particular cognitive phenomena rely on transient dynamics such as working memory and decision making [25, 26]. The idea is that brain activity is organized in spatiotemporal patterns through transient metastable states [27, 28]. For a long time the search was for a dynamic framework that describes transient reproducible and metastable dynamics. One such framework is provided by heteroclinic dynamics, for a recent review see [29]. For a review on metastable dynamics see, for example, [30].

In this paper, we demonstrate how -differently from heteroclinic dynamics- a set of deterministic equations can lead to switching dynamics, here induced by a fast change between attractive and repulsive couplings in half of the node connections, and a slow change between both types in the other half. In detail we consider an all-to-all coupling topology, but we present also results for a random network, for which we vary the density of connectivity. We briefly consider effects of non-reciprocal adaptivity when also the natural frequencies become coupling dependent.

The paper is organized as follows: In section 2 we introduce different versions of the model. Section 3 presents the results in terms of synchronization patterns as function of the model parameters, in particular of the time scales, the system size and the grid topology. Section 4 contains our conclusions. In the appendix we provide

an analytical understanding of the increasing instability with the system size.

II. THE MODEL

We consider a population of $N \geq 2$ phase oscillators, each described by its phase $\theta_i(t) \in [0, 2\pi)$, whose dynamics evolve according to a modified Kuramoto model with adaptive non-reciprocal couplings. The evolution equation for the i -th oscillator is given by

$$\dot{\theta}_i = \omega_i + \frac{1}{N} \sum_{j=1}^N k_{ij} \sin(\theta_j - \theta_i) + \xi_i(t), \quad (1)$$

where ω_i denotes the intrinsic natural frequency, and k_{ij} is the time-dependent coupling strength. The term $\xi_i(t)$ represents additive Gaussian white noise of intensity σ :

$$\langle \xi_i(t) \rangle = 0, \langle \xi_i(t) \xi_j(t') \rangle = \sigma^2 \delta_{ij} \delta(t - t'). \quad (2)$$

The coupling matrix $\mathbf{k} = [k_{ij}]$ evolves as

$$k_{ij} = \begin{cases} -\varepsilon_1 [k_{ij} + \sin(\theta_i - \theta_j + \beta_1)], & \text{for } i < j, \\ -\varepsilon_2 [k_{ij} + \sin(\theta_i - \theta_j + \beta_2)], & \text{for } i > j, \\ 0, & \text{for } i = j. \end{cases} \quad (3)$$

We choose $\beta_1 = -\frac{\pi}{2}$ and $\beta_2 = +\frac{\pi}{2}$, and $\varepsilon_1, \varepsilon_2 > 0$ are the adaptation rates for the upper and lower triangular parts of the matrix. The diagonal elements of the coupling matrix, k_{ii} , are set to zero to avoid self-coupling. This means that for connections from a lower-index oscillator i to a higher-index oscillator j , the coupling tends to adjust with a phase lag of $-\pi/2$ (Hebbian plasticity rule). For connections in the opposite direction, the adjustment follows a phase lead of $+\pi/2$ (anti-Hebbian rule). For simplicity the upper-triangular (lower-triangular) couplings k_{ij} with $i < j$ ($i > j$) are termed the upper (lower) couplings in the following. Throughout the paper we will keep the slow (fast) time scale associated with the anti-Hebbian (Hebbian) rule, respectively, since otherwise we observe only incoherent oscillations.

In most previous studies [31]-[32] the adaptation rules were chosen symmetric with $\varepsilon_1 = \varepsilon_2 > 0$. In these cases, if the phase shift was $\beta_1 = \beta_2 = +\pi/2$, the system typically remained incoherent [11], and if the phase shift was $\beta_1 = \beta_2 = -\pi/2$, two anti-phase clusters could form [11].

As stochastic extension of the standard Euler method, Equations (1) and (3) are integrated numerically using the Euler–Maruyama scheme with a fixed time step $\Delta t = 0.01$ and $\theta_i \mapsto \theta_i \bmod 2\pi$.

The initial phases $\theta_i(0)$ are sampled uniformly from $[0, 2\pi)$, while (unless stated otherwise) the initial couplings $k_{ij}(0)$ are drawn from a uniform distribution in $[-1, 1]$ with $k_{ii}(0) = 0$. The natural frequencies ω_i are in most cases set to zero, otherwise sampled from a normal distribution with a fixed mean ω_{mean} and a fixed standard deviation ω_{std} .

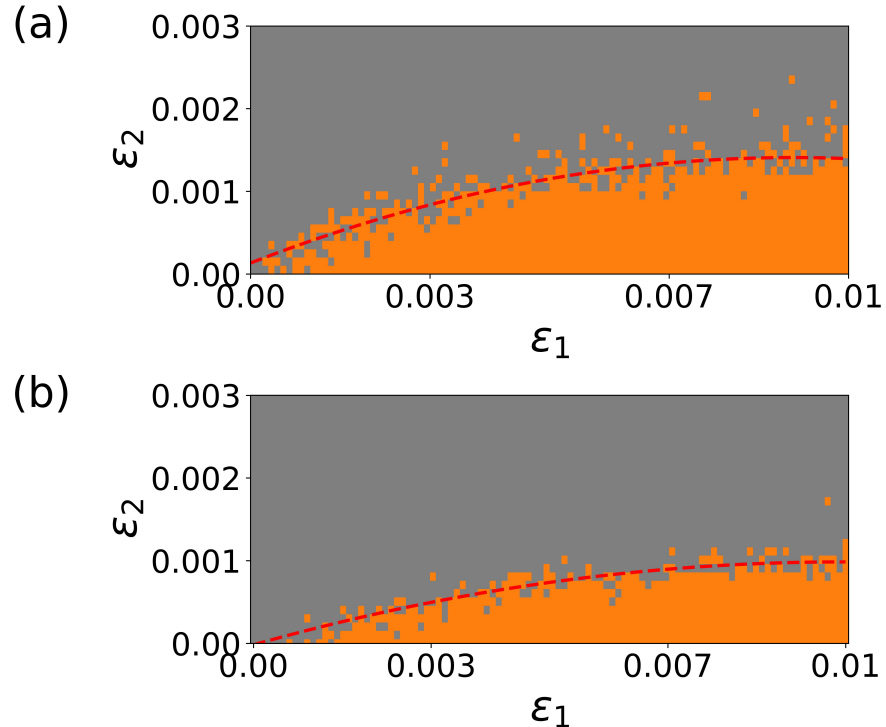


FIG. 1. Categorical heatmap of collective states as a function of (ϵ_1, ϵ_2) for (a) $N = 10$ oscillators and (b) $N = 20$ oscillators, averaged over 5 independent realizations. Colors indicate two anti-phase clusters (orange), and incoherent (gray) states; ϵ_1 is varying within $[0, 0.1]$ and ϵ_2 is varying within $[0, 0.003]$ with a step length of 0.0001. The red dashed curve should guide the eyes and roughly marks the transition boundary between two anti-phase clusters and incoherent states via a quadratic least square fit.

The degree of phase coherence is quantified using two complex quantities, the first and second Kuramoto order parameters:

$$Re^{i\psi} = \frac{1}{N} \sum_{j=1}^N e^{i\theta_j}, \quad R_2 e^{i\psi_2} = \frac{1}{N} \sum_{j=1}^N e^{2i\theta_j}, \quad (4)$$

where $R \in [0, 1]$ measures the global synchronization level, and $R_2 \in [0, 1]$ captures the presence of two anti-phase clusters. The limiting cases are as follows: $R \approx 1$ and $R_2 \approx 1$ for complete in-phase synchronization; $R \approx 0$ and $R_2 \approx 1$ for two anti-phase clusters; and both R and R_2 small for incoherent dynamics.

After an initial transient, the long-time averaged order parameters $\langle R \rangle$ and $\langle R_2 \rangle$ are computed over a sufficiently large portion of the simulation succeeding the transient. As we will see, for our results it is sufficient to classify the collective states as follows: if $\langle R \rangle$ and $\langle R_2 \rangle$ both are greater than a threshold R_{th} , the system is in the in-phase synchronized state. If $\langle R \rangle$ is less than or equal to R_{th} , and $\langle R_2 \rangle$ is greater than R_{th} , the system is in the two anti-phase clusters state. In all other cases, the system is considered incoherent. For the threshold we have chosen $R_{th} = 0.8$, though usually for anti-phase synchronized clusters $R_2 > 0.8$.

III. RESULTS

We start with a discussion of the typical stationary states and argue for the choice of parameters which we keep throughout this paper. Next we analyze features of randomness in spite of deterministic dynamics, the dependencies on the initial conditions, the system size, and the effect of disorder. In the last two subsections we consider different versions of the generalized Kuramoto model.

A. Stationary states and choice of parameters

To visualize the dependence of collective states on the adaption rates (ϵ_1, ϵ_2) , we perform numerical simulations of the coupled system (1)-(3) with $N = 10$ and $N = 20$ oscillators over multiple realizations.

The simulations are carried out in the noise-free case with identical intrinsic frequencies $\omega_i = 0$ for all oscillators $i = 1, \dots, N$. To track the long-time dynamics, the order parameters, R and R_2 , are computed and averaged over the last sufficiently long time window. Each parameter pair (ϵ_1, ϵ_2) is simulated for 5 independent realizations, and the resulting mean order parameters $\langle R \rangle$ and $\langle R_2 \rangle$ are used to classify the collective state.

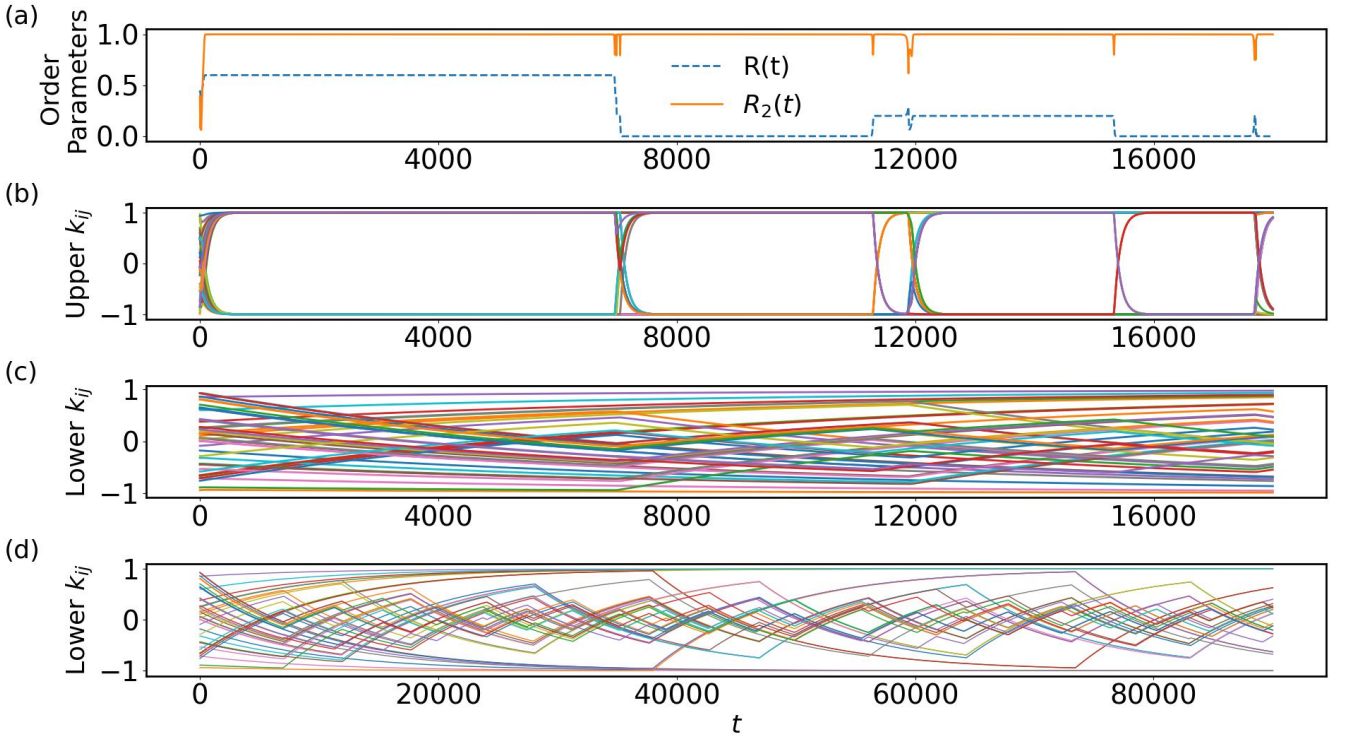


FIG. 2. (a) Time series of the first- and second-order Kuramoto order parameters $R(t)$ (dashed line) and $R_2(t)$ (solid line) for $\varepsilon_1 = 0.01$ and $\varepsilon_2 = 0.0001$ with $N = 10$. After initial convergence to $R_2 \approx 1$, occasional deviations occur, visible in spikes, which subsequently return to the same state. (b-c) Upper part of the couplings k_{ij} (for $i < j$) and lower part of k_{ij} (for $i > j$). As soon as R_2 deviates from 1, a few oscillators switch clusters, which leads to changes in the slopes of the corresponding k_{ij} values. Since $\varepsilon_1 = 0.01$ is significantly larger than $\varepsilon_2 = 0.0001$, the upper k_{ij} values quickly reach their equilibrium values of ± 1 , whereas the lower k_{ij} values adjust more slowly. (d) Extended time view of (c) to see some structure in the evolution of the lower couplings.

The resulting categorical heatmap is shown in Fig. (1). Each pixel corresponds to a $(\varepsilon_1, \varepsilon_2)$ pair, color-coded by the observed collective state. Since $\varepsilon_2 > 0$ corresponds to the anti-Hebbian coupling, it tends to disrupt phase coherence, and sufficiently large values of ε_2 generally lead to incoherent dynamics. In contrast, when $\varepsilon_1 \gg \varepsilon_2 > 0$, the upper-triangular Hebbian interactions dominate, promoting the formation of two anti-phase clusters for most parameter realizations.

To examine the dynamics in detail, we simulate the system (1)-(3) with $N = 10$ oscillators, noise intensity $\sigma = 0$ and intrinsic frequencies $\omega_i = 0 \forall i$. We fix the coupling parameters at $\varepsilon_1 = 0.01$ and $\varepsilon_2 = 0.0001$, a regime where two anti-phase clusters are expected from Fig. (1) (a). While one might anticipate that R_2 would converge to one after an initial transient, we observe metastable behavior: R_2 initially approaches 1, then occasionally deviates from this value, only to return to $R_2 \approx 1$ after a few iterations. We have seen the same recurrent deviations of R_2 as shown in Fig. (2) (a) also over a total integration time of up to 9×10^7 steps.

As seen in Fig. (2) (a), also the standard Kuramoto order parameter R shows metastable behavior. Depending on the degree of synchronization, the value of R after a spike

may be different, and whenever R_2 is perturbed, R experiences a corresponding disturbance. During $R_2 = 1$, the two anti-phase clusters remain well separated by a phase difference of π , although the number of oscillators in each cluster may vary temporarily during the disturbances of R_2 . After a spike in R_2 , the system returns to a state with $R_2 \approx 1$, preserving the two-cluster structure with π phase difference. Thus, a spike in the order parameter R_2 indicates a short deviation from the organization into two anti-phase synchronized clusters which obviously corresponds to an unstable solution.

It is instructive to plot the evolution of the asymmetric coupling matrix k_{ij} in Fig. (2) (b-c). In panel (b), we observe the time evolution of the upper part k_{ij} for $i < j$. As the system evolves, some of the couplings settle temporarily at $+1$, while others stabilize temporarily at -1 . However, when R_2 deviates from 1, there are switches in some of the k_{ij} values from $+1$ to -1 or vice versa, indicating a temporary departure from the anti-phase synchronized two-cluster state. At the same time, some of the lower couplings k_{ij} for $i > j$ also undergo slope changes, as shown in panel (c), but evolving on a much slower time scale. Panel (d) displays the evolution of the lower couplings on a long time scale,

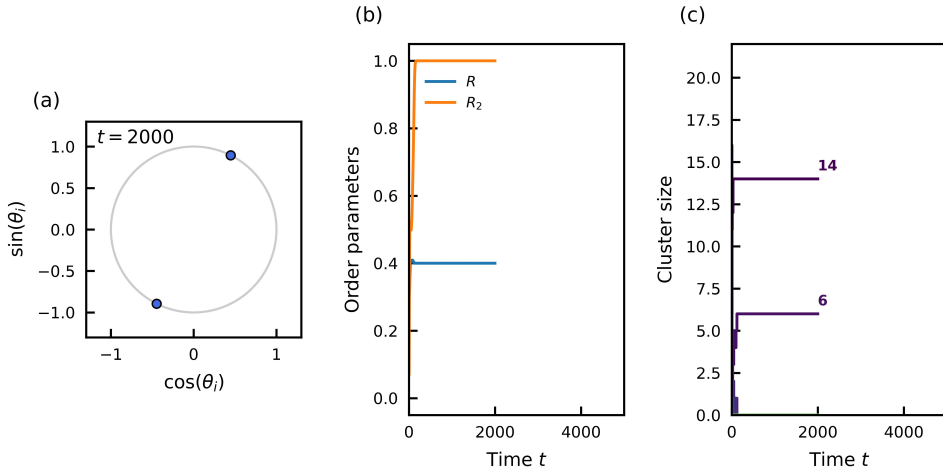


FIG. 3. Snapshots at $t = 2000$ of the phases (a), the order parameters R and R_2 (b) and the cluster sizes (c) before a switching event for $N = 20$.

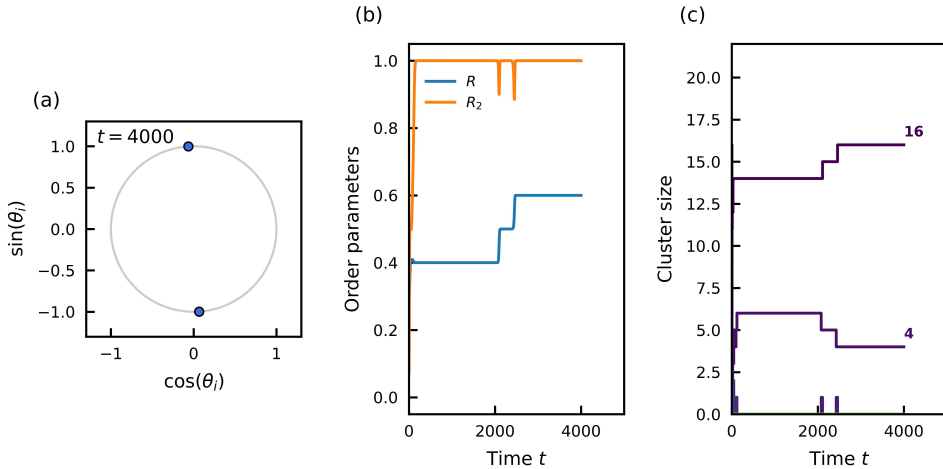


FIG. 4. Same as Fig. 3, but snapshot at $t = 4000$ after a switching event. Note that the cluster sizes have changed to a different partition before and after the switching of oscillators. In both panels (a) and (b), two anti-phase clusters are visible, each perfectly synchronized.

where it is seen more clearly that not all couplings are affected by a switch of R_2 and one may wonder whether some periodic structure is seen on long time scales.

Metastability is the essential novel feature that we observe in these combinations of non-reciprocal couplings with respect to their sign and time scales. It is absent in the symmetric case [11]. Even, when $\varepsilon_1 \gg \varepsilon_2$ with $\varepsilon_1 = 0.01$, $\varepsilon_2 = 0.0001$, but $\beta_1 = \beta_2$, the system does not exhibit metastability. In this case, when $\beta_1 = \beta_2 = -\frac{\pi}{2}$, two stable anti-phase clusters emerge, while for $\beta_1 = \beta_2 = +\frac{\pi}{2}$, oscillations are only incoherent. Metastability, on the other hand, is observed in our system when there is sufficient asymmetry in the adaptive coupling dynamics, specifically when $\varepsilon_1 \gg \varepsilon_2 > 0$, as shown in the orange-colored region of Fig. (1) as well as $\beta_1 \neq \beta_2$. The slow dynamics adds as a perturbation on the fast dynamics; for the fast dynamics alone we

would see a dynamic realization of Harari's theorem [33]. According to that, the set of all points a balanced signed graph can be partitioned into two disjoint sets such that each positive line joins two points of the same subset and each negative line joins two points from different subsets. In our case, positive lines are realized as upper couplings within the same cluster and negative lines as upper couplings between the other cluster. The two anti-phase synchronized clusters are then perturbed by the slow dynamics which is manifest in some oscillators changing their cluster affiliation from time to time.

Numerically we confirm that occasionally some oscillators switch groups, causing R_2 to deviate from 1. After a few steps, these oscillators return to a possibly slightly different anti-phase cluster configuration, and R_2 revisits the value of 1. The number of oscillators in each cluster may change with each deviation of R_2 from 1. Here, we

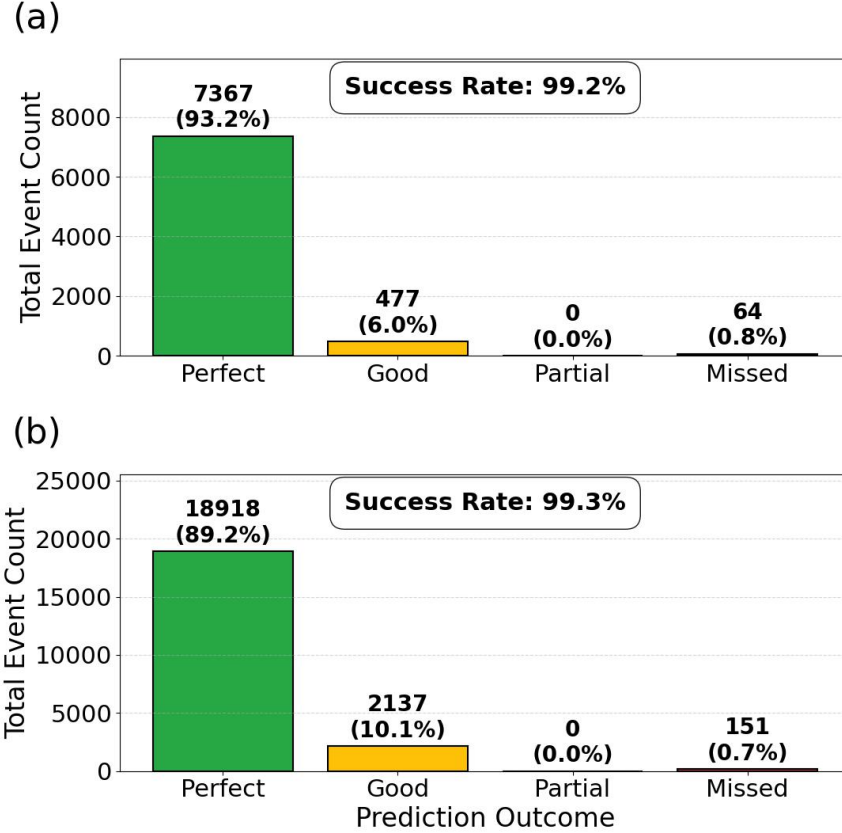


FIG. 5. Snapshot-based prediction performance across 1,000 random realizations for (a) $N = 6$ and (b) $N = 10$. The bars represent the total count of switching events categorized by prediction accuracy. The percentage shown above each bar indicates the frequency of that outcome relative to the total number of detected events. The overall success rate (combined *Perfect* and *Good* categories) remains remarkably stable as the system size increases.

include four videos [34] for different system sizes, $N = 20$ and $N = 200$, demonstrating these features, in particular how the group sizes may change with each spike in R_2 . In Figs. 3 and 4 we include snapshots of these movies before and after a spike in R_2 . What causes the changes in the slope of fast and slowly evolving couplings and which couplings are affected? Let us consider the simplest case, where a single oscillator l changes its cluster affiliation. What happens to the couplings k_{lk} in which this oscillator is involved? From the evolution of the coupling strengths k_{ij} given in Eq. (3) it is seen that two oscillators with indices l and k , chosen from the N oscillators, which initially belong to the same cluster at time $t = t_1$ in an anti-phase cluster configuration with $R_2 = 1$ evolve as

$$\begin{aligned} \dot{k}_{lk} &= -\varepsilon_1 (k_{lk} - 1), & \text{for } l < k, \\ \dot{k}_{lk} &= -\varepsilon_2 (k_{lk} + 1), & \text{for } l > k. \end{aligned}$$

Since $k_{lk} \in [-1, 1]$ and $\varepsilon_1, \varepsilon_2 > 0$, these relations imply $\dot{k}_{lk} \geq 0$, for $l < k$, and $\dot{k}_{lk} \leq 0$, for $l > k$. Thus, when oscillators l and k are in the same cluster, the

upper-triangle elements of the coupling matrix ($l < k$) increase toward $+1$, while the lower-triangle elements ($l > k$) decrease toward -1 . Now suppose that at time $t = t_2 > t_1$, oscillator l switches its affiliation to the opposite cluster, so that now $\theta_l - \theta_k = \pi$. In this case, the coupling dynamics becomes

$$\begin{aligned} \dot{k}_{lk} &= -\varepsilon_1 (k_{lk} + 1), & \text{for } l < k, \\ \dot{k}_{lk} &= -\varepsilon_2 (k_{lk} - 1), & \text{for } l > k. \end{aligned}$$

and, because $k_{lk} \in [-1, 1]$, we obtain $\dot{k}_{lk} \leq 0$, for $l < k$, and $\dot{k}_{lk} \geq 0$, for $l > k$.

In conclusion, this analysis shows that as long as two oscillators are in the same cluster, which is a metastable configuration, the couplings k_{lk} evolve toward the saddle-equilibrium $\dot{k}_{lk} = 0$ with either positive or negative slope. However, when one of the oscillators switches to the opposite cluster, the sign of the phase difference changes by π , and the slope of evolution of k_{lk} reverses. Due to the difference in time scales this happens fast for upper couplings and very slowly for lower ones, so slowly that

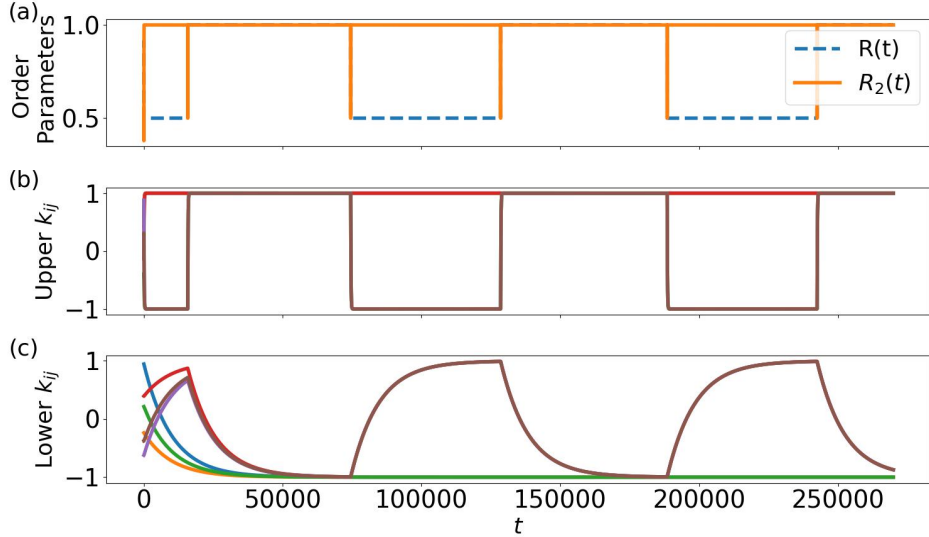


FIG. 6. Periodic and synchronized evolution not only of phases (a), but also of upper and lower couplings into one or two clusters for a network of $N = 4$ oscillators with only one saddle. Other parameters as in Fig. 2.

the lower couplings do not reach the equilibrium values of $\dot{k}_{lk} = 0$ before the next switch happens.

Numerically and visible in the attached movies we observe that depending on the system size, for small sizes $N = 10$ or $N = 20$, it is one or a few oscillators that change their cluster affiliation at the spikes of R_2 , for larger sizes these are more. What is typical in the movies is the splitting into two clusters of similar size as well as the fact that only a few oscillators change their affiliation. This reminds to “weak ties” in social systems, where a few members of a community are weakly bound and willing to switch their community (of shared opinions, for example), while the majority is strongly bound, and the weak ties are of beneficial impact on the system, as analyzed by Gronevetter [35]. The reason why oscillators change their cluster affiliation is determined by the attractor landscape and the saddles generated by the dynamics of Eqs. 1-3 that we analyze in section III D. In brain dynamics this would correspond to oscillatory units which easily switch the group with which they synchronize.

B. Features of randomness

The time evolution of the order parameters looks like generated by a stochastic source in spite of the fully deterministic dynamics of Eqs. 1-3. The events when one or more oscillators change their cluster affiliation look randomly distributed. The only source of randomness is the quenched distribution of initial phases and couplings which determine the initial distance of the phases from the saddle equilibria and therefore their trajectories through attractor space. Actually, on an intermediate time scale of the order of the interval between two switch-

ing events, the distance from the next saddle is essential to predict which oscillator escapes first in a next switching event. Assuming that there is a switch at time t of one or a few oscillators and that we know the instantaneous phase velocities $\dot{\theta}_i$ at an earlier time $t_{\text{snap}} = t - \tau_{\text{win}}$ from a snapshot at that time, we approximate the estimated time of escape (ETE) for each oscillator i as

$$\eta_i = \frac{|\theta_B - \theta_i(t_{\text{snap}})|}{\dot{\theta}_i(t_{\text{snap}}) dt}. \quad (5)$$

Here θ_B is chosen as π . This choice is motivated by the circular topology of the phase space: π marks the point of maximum phase separation from the origin (0 or 2π), and crossing it signals a definitive change in cluster membership, since we have two anti-phase synchronized clusters. $\dot{\theta}_i(t_{\text{snap}}) dt$ represents the phase displacement per simulation increment at the time of the snapshot, so the ratio on the right-hand side gives the time in units of simulation steps it takes oscillator i to overcome distance $\theta_B - \theta_i(t_{\text{snap}})$. This time is minimal for the oscillator i^* which is the first to change its cluster affiliation.

$$i^* = \arg \min_i (\eta_i). \quad (6)$$

Note that the snapshot of velocities $\dot{\theta}_i(t_{\text{snap}})$ depends on the upper and lower couplings which coevolve with the phases. However, our previous figures for k_{ij} show that within two switching events upper couplings are almost constant, as they converge fast to their equilibrium values, and lower couplings are so slow that their change may be neglected. Moreover, the distance is assumed to increase linearly with time. Nevertheless this approximation works quite well to predict the dynamics after a switch including an identification which oscillator will

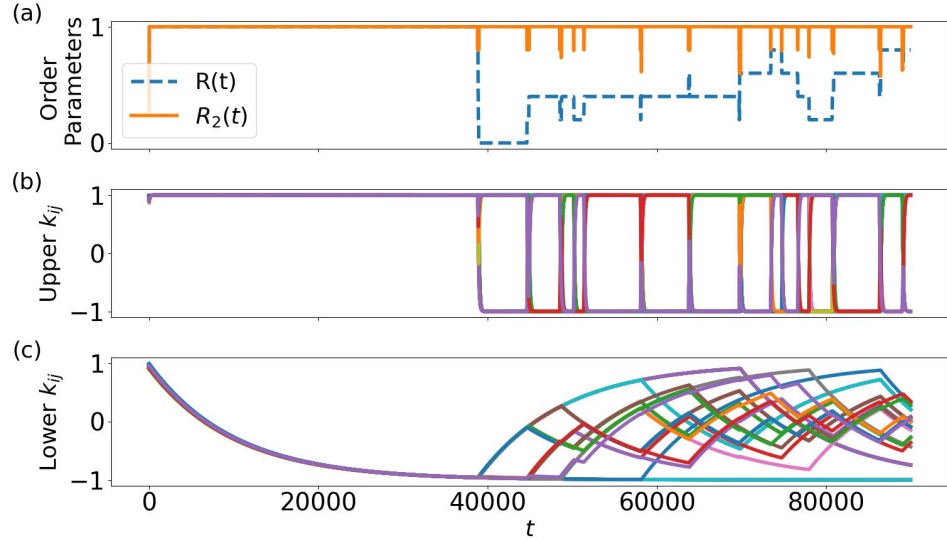


FIG. 7. Dependence on the initial conditions for upper and lower couplings, here both chosen from a distribution of k_{ij} close to $+1$. Note that the first long transient corresponds to a fully synchronized solution, observed very rarely as transient.

switch first. Before we discuss the concrete results, some remarks are in order about the choice of τ_{win} , $\tau_{\text{win}} = 200$ turns out to be a good choice, given the other parameters. If τ_{win} is chosen too large, the co-evolution of couplings can no longer be neglected, oscillators whose ETE exceeds a cutoff value $\eta_{\text{max}} = 500$ steps are excluded from consideration. If τ_{win} is too short, there is no prediction. If more than one oscillator switches its cluster affiliation, we group individual switches that happen very close together into a single collective event. If several oscillators overcome the distance of π within 50 simulation steps of each other, they are evaluated as a single event. For entire groups changing their affiliation, we predict the membership of the switching cluster \mathcal{P} by including any oscillator j whose ETE lies within a temporal margin $\Delta\eta$ of the ‘leading oscillator’ i : $\mathcal{P} = \{j \mid \eta_j \leq \eta_{i^*} + \Delta\eta\}$. This margin accounts for the finite temporal spread of collective switching events and is set to $\Delta\eta = 150$ steps in our simulations, based on the typical duration of observed group switching.

By comparing the predicted set \mathcal{P} with the actual set of oscillators \mathcal{A} that overcome a distance of π at time t , predictions are classified into four categories: Perfect: $\mathcal{P} = \mathcal{A}$. The predicted group exactly matches the actual switchers. Good: $\mathcal{A} \subset \mathcal{P}$. All actual switchers were identified, but additional oscillators were incorrectly included. Partial: $\mathcal{P} \cap \mathcal{A} \neq \emptyset$ but $\mathcal{A} \not\subset \mathcal{P}$. Some switchers were correctly identified, while others were missed. Missed: $\mathcal{P} \cap \mathcal{A} = \emptyset$. No actual switchers were identified. To skip initial transient behavior, only switching events occurring after $t > 0.3 T_{\text{total}}$ are included from overall $T_{\text{total}} = 1.8 \times 10^6$ steps.

The performance of our snapshot-based prediction is summarized in Fig. 5 for both $N = 6$ and $N = 10$ nodes. For the $N = 6$ configuration (Fig. 5 (a)), the framework

achieved an overall success rate of 99.2%, with 93.2% of events classified as *Perfect*. This indicates that the instantaneous state 200 steps prior to a switch contains nearly all the information required to identify the switching cluster. As the system size increases to $N = 10$ (Fig. 5 (b)), the predictive robustness is maintained with a success rate of 99.3%. Interestingly, while the proportion of *Perfect* predictions remains high at 89.2%, there is a slight increase in the *Good* category (10.1% compared to 6.0% in the $N = 6$ case). This shift suggests that in larger coupled systems, the ‘lead’ oscillator exerts a stronger influence on its neighbors, occasionally causing the inclusion of ‘follower’ oscillators in the predicted set \mathcal{P} that do not quite reach θ_B within the expected window. The zero occurrence of *Partial* predictions across all realizations demonstrates that the temporal margin $\Delta\eta = 150$ is very effective at capturing events where more oscillators are involved. Furthermore, the consistently low rate of *Missed* events ($< 1\%$) confirms that cluster transitions in the adaptive Kuramoto model are predictable within an intermediate time scale. Our approach relies exclusively on a single temporal snapshot of the system state. What cannot be predicted is the new partition into two clusters after the switching event and the dynamics on a long-time scale. One might be interested in the probability that a given set of oscillator phases find the same couplings (actually coupling conditions for their own evolution) after some possibly long time, as the evolution -locally in time- looks random. The question for finding repeatedly the same conditions is the question for long-time periodicity. Such long periods in the Kuramoto order parameter from short period oscillations have been observed in [36]. For larger networks we cannot answer this question, but for a system of $N = 4$ oscillators, the six upper couplings and the six lower couplings synchro-

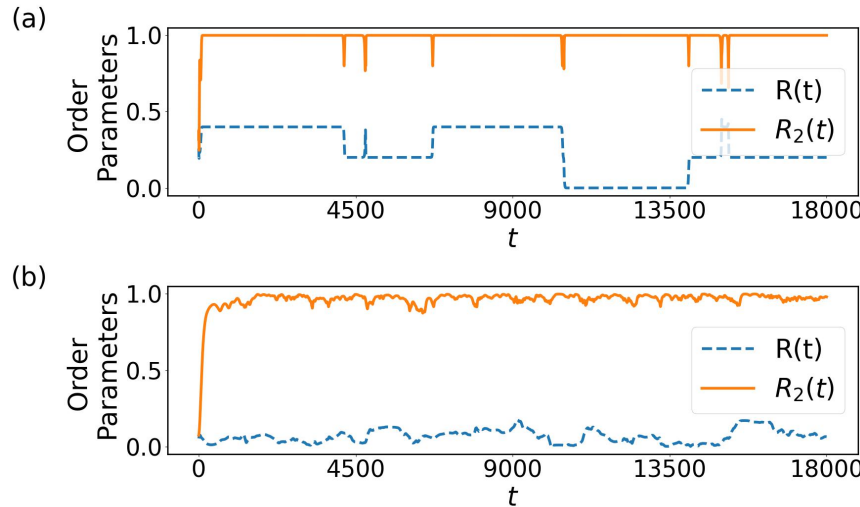


FIG. 8. Dependence on the system size for (a) $N = 10$ and (b) $N = 200$ oscillators with the same parameters as in Fig. (2). Compared to the smaller system ($N = 10$), the fluctuations in R_2 are more frequent, indicating a larger instability, but less pronounced in size, that is, smaller deviations from the anti-phase synchronized clusters for $N = 200$. Still, all values of R_2 remain close to one, corresponding to an organization into two anti-phase clusters.

nize into one or two clusters, as well as the phases, for $N = 4$ as for $N = 3$ the system has only one saddle point and the evolution of all couplings is strictly periodic, see Fig. 6.

In summary, on intermediate time scales it is the momentary distance from π of the phase position and the phase velocity at that instant of time, which allow a prediction of which oscillator (group of oscillators) will escape next, knowing that there is an escape event. As soon as this distance is overcome, we can be sure to be in the attraction regime of the other cluster. It is the random initial conditions which determine the initial phase position and lead to an ensemble of time evolutions unless identical initial conditions are chosen via the same seed. Given a set of fixed initial conditions, the waiting time distribution between two switches of the order parameter R_2 looks random on longer time scales, unless it happens to become periodic. We address this irregularity to the complex attractor landscape that allows the escape from saddles and determines the entrance to the attraction regimes of new saddles.

C. Choice of initial conditions and natural frequencies

Before we discuss the stability properties as a function of the system size, some remarks are in order about the choice of initial conditions and the values of the natural frequencies. If we keep all other parameters the same and set the intrinsic frequencies ω_i to a homogeneous nonzero value, e.g., $\omega_i = 3$, we observe that the phases θ_i oscillate over time with constant phase difference of π between the temporarily forming two anti-phase synchronized clus-

ters, otherwise the main features of metastability remain qualitatively the same as for $\omega_i = 0$. This is expected as we can go to a co-rotating frame and transform the system to zero frequency.

If we choose uniformly distributed initial configurations for upper and lower couplings very close to 1, this choice results in some delay of the onset of metastable dynamics, where for the upper couplings it is the fully synchronized state that is stable until metastability sets in, see Fig. 7.

D. Metastability as a function of the system size

In Fig. 8 we compare the evolution of the order parameters as a function of the system size for $N = 10$ in Fig. 8 (a) and $N = 200$ in Fig. 8 (b).

For $N = 200$ the distinction between transient stable configurations interrupted by short excursions to other clusters becomes less pronounced. The movie of [34] for $N = 200$ shows the evolution of phases, snapshots are given in Figs. 9 and 10 before and after a spike in R_2 . We still see remnants of an organization into two anti-phase synchronized clusters, where on short time scales always some oscillators escape and return to their cluster, more frequent are the events where the escape succeeds over a distance π in the phases. At intermediate times also configurations with several coexisting clusters are forming, leading to stronger spikes in R_2 .

To understand more quantitatively the increasing instability with the system size, we summarize in the following the stability analysis which is detailed in the Appendix. For the fully connected Kuramoto model with $\omega_i = 0$ and $\sigma = 0$ we start from a two-cluster anti-

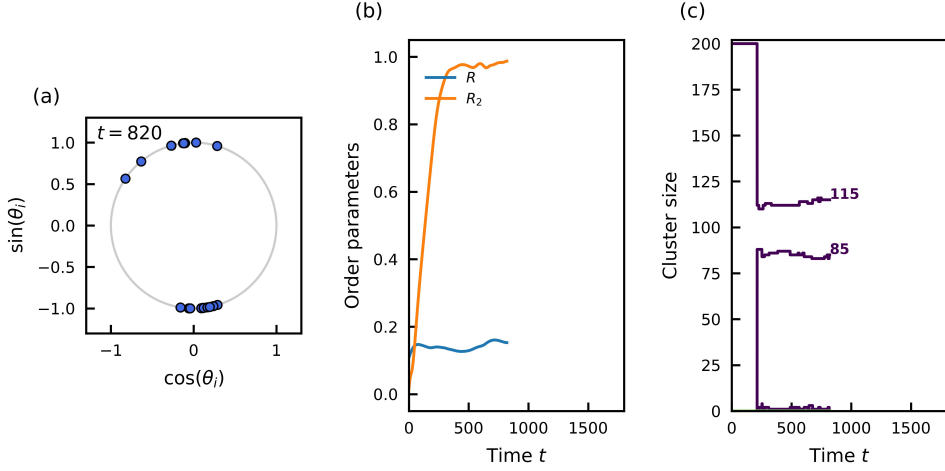


FIG. 9. Same as Fig. 3, but for $N = 200$. Note that two anti-phase clusters are less perfectly synchronized than for $N = 20$. The partition into two clusters is roughly half-half.

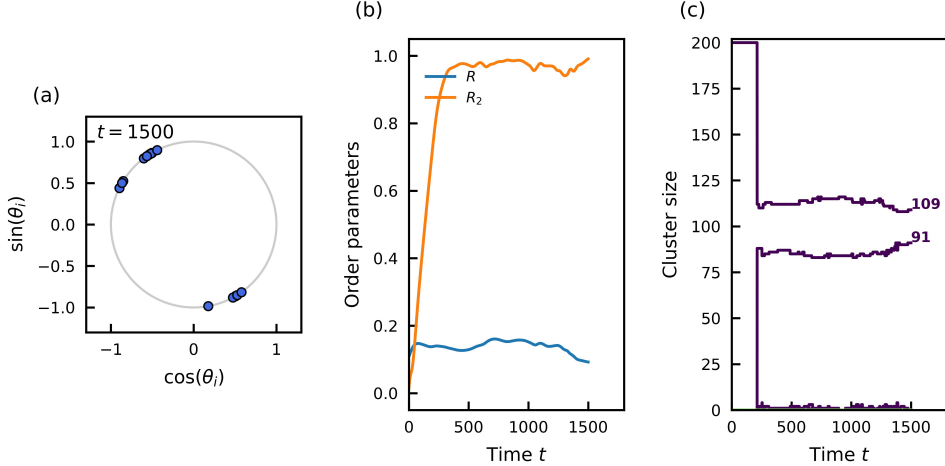


FIG. 10. Same as Fig. 4, but for $N = 200$. The size of the two clusters of the partition varies only slightly before and after the switch, but as compared to $N = 20$, more and more oscillators are involved in changing their cluster affiliation.

phase synchronized solution with clusters A and B of size N_A and N_B . Next we perform a stability analysis around the two-cluster solution. The Jacobian takes a block form with four blocks $J_{\theta\theta}$, $J_{\theta k}$, $J_{k\theta}$, and J_{kk} . For the phase-coupling block $J_{\theta k}$ it is easy to show that the matrix vanishes. Therefore the determinant of the entire Jacobian factorizes into those of the diagonal entities $\det J_{\theta\theta} \det J_{kk}$, and the eigenvalues are the union of those of $J_{\theta\theta}$ and J_{kk} . The eigenvalues of J_{kk} turn out to be all negative. Thus the problem is reduced to determine the eigenvalues of $J_{\theta\theta}$. At the two-cluster anti-phase equilibrium the couplings attain their equilibrium values $\dot{k}_{ij} = 0$, which leads to vanishing row sums and one zero eigenvalue, corresponding to the global phase shift of the two-cluster solution. Moreover, it can be shown that $\chi J_{\theta\theta} \chi = -J_{\theta\theta}$ with a flip matrix χ . Therefore the eigenvalues of $J_{\theta\theta}$ occur in symmetric pairs with $m - 1$ positive values $\lambda_k = 1 - 2k/N$, $k = 1, 2, \dots, m - 1$ and $m - 1$

negative values $\lambda_{-k} = -(1 - 2k/N)$, $k = 1, 2, \dots, m - 1$ for $N = 2m$ plus 2 zero eigenvalues; for $N = 2m + 1$ we have m positive and m negative values and one zero eigenvalue, λ_k, λ_{-k} as before with $k = 1, 2, \dots, m$. This proves that with increasing system size N , we have an increasing number of unstable directions for the two anti-phase synchronized cluster solution.

E. Impact of disorder via noise or natural frequencies

In Kuramoto models with two non-reciprocally interacting populations, disorder in the frequencies or noise can stabilize a chiral phase, which is chiral in the sense that instead of static phase alignment a chiral motion is observed such that in spite of zero natural frequencies, oscillations spontaneously rotate either clockwise

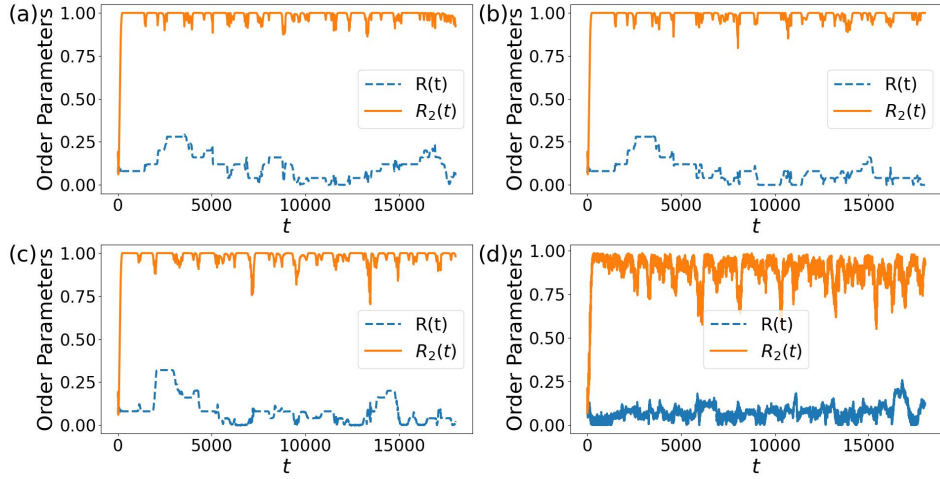


FIG. 11. Time evolution of the order parameters R and R_2 for four noise strengths: (a) $\sigma = 0$, (b) $\sigma = 0.00001$, (c) $\sigma = 0.001$, (d) $\sigma = 0.1$, leading to incoherent oscillations underlying R and R_2 in (d). Parameters $N = 50$, others as in Fig. 2. We use the same random initial conditions to generate the four figures in panel (a)-(d). For further comments see the main text.

or anti-clockwise [23]. In our version of the Kuramoto model with one population and adaptive non-reciprocal couplings to all other oscillators, the role of disorder or noise that we observed is toward an increase of escapes from a two anti-phase synchronized cluster state. For the strongest noise amplitude in Fig. 11 (d), the order parameter R_2 shows larger deviations from 1, indicating that temporarily several clusters have formed, but R_2 remains close to 1 and returns to this value again and again, so that still remnants of the anti-phase synchronized two clusters are still visible. Since the phase difference between the two clusters is roughly π , noise is in general not sufficient for an escape where many oscillators overcome the distance and change their cluster affiliation at the same time, just a few succeed as the panels (c) in Fig. 9 and 10 show. In particular, noise does not improve synchronization at an intermediate noise level; due to a large phase difference, it monotonically weakens the perfect anti-phase cluster synchronization, allowing for longer escapes, and broadens a bit the in-phase synchronization within a cluster.

F. Effects of a sparse network topology

In the next version of the model inspired by the Ref. [12], the dynamics of the oscillators and their adaptive couplings have been modified to account for a connected but sparse random network topology. The coupling matrix k_{ij} now evolves only along the links of a network represented by the adjacency matrix $A = [A_{ij}]$. The phase dynamics are therefore weighted by the network structure:

$$\dot{\theta}_i = \omega_i + \frac{1}{\sum_j A_{ij}} \sum_{j=1}^N A_{ij} k_{ij} \sin(\theta_j - \theta_i), \quad (7)$$

where $\sum_j A_{ij}$ is the degree of node i . The adaptive evolution of the coupling matrix is modified such that only links, which are already initially existing, update according to the asymmetric rules:

$$k_{ij} = \begin{cases} -\varepsilon_1 [k_{ij} + \sin(\theta_i - \theta_j - \frac{\pi}{2})] A_{ij}, & i < j, \\ -\varepsilon_2 [k_{ij} + \sin(\theta_i - \theta_j + \frac{\pi}{2})] A_{ij}, & i > j, \\ 0, & i = j. \end{cases} \quad (8)$$

Using the dynamics (7)-(8), we simulated networks of size $N = 10$ over multiple realizations for varying average degrees $\langle k \rangle$. The lifetime of the two-cluster anti-phase state was computed by monitoring the order parameters R and R_2 , identifying periods where $R < R_{\text{th}}$ while $R_2 > R_{\text{th}}$.

Figure (12) shows the mean and standard deviation of the two-cluster lifetimes over 100 realizations as a function of the average degree $\langle k \rangle$. As $\langle k \rangle$ increases and the network becomes more densely connected, on average the dwell time increases and the metastability is more pronounced. The network topology introduces fluctuations in the dwell times across realizations, reflected in the error bars. Using our rough synchronization threshold of 0.8, we do not see a pronounced rearrangement of clusters of the synchronized oscillators, differently from [12], in our case the two anti-phase cluster configuration is quite dominant.

G. Kuramoto Model with non-reciprocal and adaptive frequencies

Reciprocal synaptic plasticity alone can have the interesting effect that heterogeneous layered clusters with different frequencies emerge from homogeneous populations as the Fourier zero modes of the phase coupling function is included, leading to an additional constant

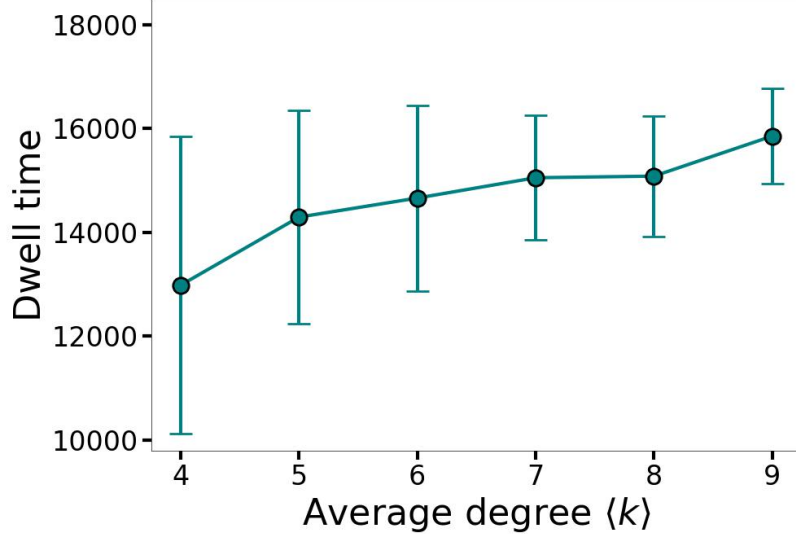


FIG. 12. Increase of the dwell time in the vicinity of saddles with the network connectivity. The metastability is most pronounced for a fully connected network with average degree $\langle k \rangle = 9$ and $N = 10$.

term in the interaction part of the oscillators [13]. Here we implement a Kuramoto model, inspired by the framework outlined in [13], but with asymmetric plasticity. In this model, the frequency of each oscillator, denoted by $\tilde{\omega}_i$, depends on the coupling strengths, which evolve dynamically over time. The frequency of the i -th oscillator is given by the following equation:

$$\tilde{\omega}_i = \omega_i + \frac{\Gamma_0}{N} \sum_{j=1}^N k_{ij}, \quad (9)$$

where $\Gamma_0 \in [0, 1]$ is a constant that influences the phase dynamics between oscillators. The phase evolution for each oscillator is governed by the equation:

$$\frac{d\theta_i}{dt} = \omega_i + \frac{1}{N} \sum_{j=1}^N k_{ij} (\Gamma_0 - \sin(\theta_i - \theta_j + \alpha)), \quad (10)$$

where α is a constant that modulates the coupling strength between oscillators. The coupling matrix k_{ij} now evolves according to the non-reciprocal plasticity rule as defined by Eq. (3), with $\beta_1 = -\frac{\pi}{2}$ and $\beta_2 = +\frac{\pi}{2}$. Initially, we set $\alpha = 0$, which simplifies the model to the noiseless version of the proposed model (1) with $\Gamma_0 = 0$. Even when the initial natural frequencies ω_i are set to zero, a nonzero Γ_0 ensures that the frequencies $\tilde{\omega}_i$ remain time-dependent. This leads to incoherent oscillations among frequencies. Furthermore, when Γ_0 is nonzero, the phases θ_i of the oscillators also evolve, and again we observe metastability in the system. This metastable behavior persists for values of Γ_0 in the range $[0, 0.2]$.

At small nonzero values of $\alpha \in [-0.04, 0.04]$, we observe the formation of two distinct clusters, with a phase difference of approximately π between them. As Γ_0 increases

to the range $(0.2, 0.6)$, the system still maintains two phase-locked clusters, but the phase difference between them is typically less than π . When Γ_0 exceeds 0.6 and lies in the range $[0.6, 1]$, the oscillators become fully incoherent, and no phase locking is observed.

The time evolution of the order parameters and upper and lower couplings looks qualitatively the same as before. Whenever R_2 approaches 1, the oscillators' phases naturally divide into two groups. Despite all oscillators starting with $\omega_i = 0$, they begin to oscillate due to the nonzero value of $\Gamma_0 = 0.1$. We show a snapshot at $t = 15000$ of the phases and frequencies $\tilde{\omega}_i$ in Fig. (13) (a) and (b), where each oscillator has a distinct $\tilde{\omega}_i$ that oscillates over time. The 10 oscillators are divided into two groups separated by a phase difference of π , although the frequencies are quite heterogeneous. In panel (c), we display a snapshot of the coupling matrix k_{ij} . The lower triangle of the matrix does not yet converge to its equilibrium values of ± 1 due to the slow adaptation rate $\varepsilon_2 = 0.0001$, the upper one does. One can easily read off which oscillators remain in the same cluster with upper couplings being attractive and which ones are in opposite clusters with upper couplings being repulsive. The long-time evolution of the phases θ_i (Fig. (13) (e)) indicates how the anti-phase synchronization patterns of phases change together with the frequency patterns (d) in time intervals between abrupt changes of the slope of $\tilde{\omega}_i$ and θ_i . Note that $\tilde{\omega}_i$ play the role of effective natural frequencies. Obviously they can considerably differ from the actual frequencies θ_i , being larger in the time interval between $t \in [2000, 4000]$ than in the one between $t \in [8000, 10000]$, although the opposite order is seen for $\tilde{\omega}_i$.

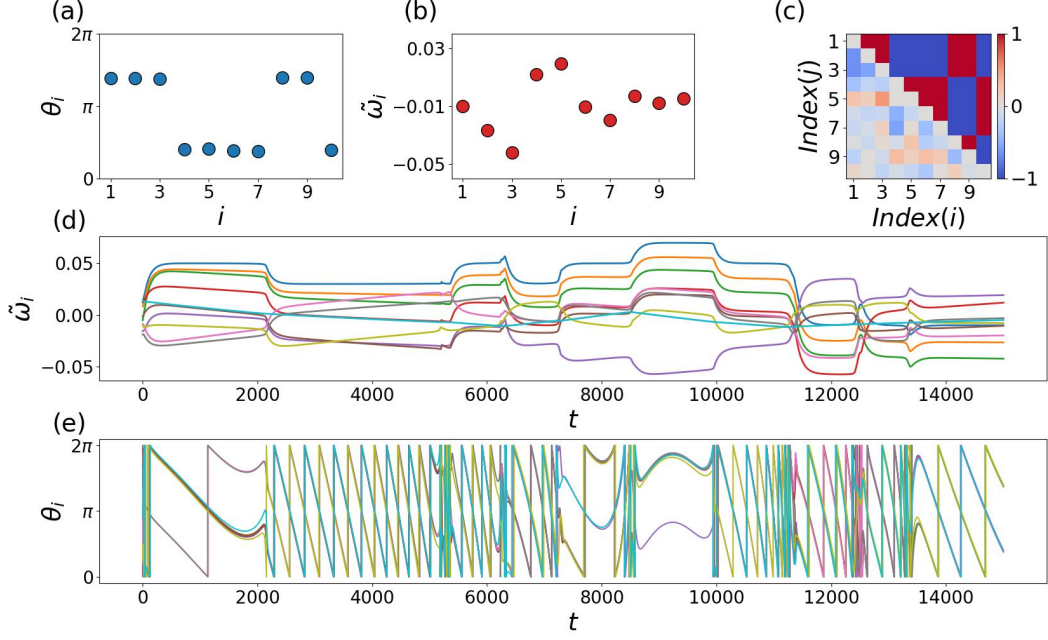


FIG. 13. When frequencies become coupling dependent. Panel (a) shows a snapshot of the two anti-phase clusters of the oscillator phases. Panel (b) displays the instantaneous frequencies at the same snapshot time $t=15000$, revealing incoherent frequency dynamics. The evolution of the couplings is shown in panel (c), where the upper couplings rapidly reach their equilibrium values of ± 1 , while the lower couplings fail to do so. Panel (d) presents the time evolution of the frequencies over a longer time interval, and panel (e) shows the corresponding long-time evolution of the phases. Further details are discussed in the main text.

IV. CONCLUSIONS AND OUTLOOK

We have studied generalized Kuramoto models of classical oscillators which have applications in particular to model oscillatory dynamics in neuronal networks. Strengths or weights assigned to synapses are in general not symmetric, therefore it is natural to model their dynamics via non-reciprocal couplings, where we have chosen Hebbian and anti-Hebbian rules for adaptation. Moreover, the time scales on which adaptation takes place need not be the same in both directions. For a certain range of parameters and in this combination of asymmetric coupling's type and time-scale, we observe metastability of (in general) two anti-phase clusters of synchronized oscillators where a few oscillators (“switcher oscillators”) change their cluster affiliation. This is induced by a dynamical switch of the coupling type (attractive or repulsive) of connections ij to nodes j from swing oscillators i , which happen on different time scales, depending on whether $i < j$ or $i > j$. We have seen temporary remnants of dynamical realizations of Harari's theorem, that is, the existence of two anti-phase synchronized clusters on an all-to-all topology, as long as the dynamics on the second time scale, parameterized by $1/\epsilon_2$, can be neglected.

In view of brain dynamics it is of interest to identify in-

teractions which are Hebbian-like in one direction and anti-Hebbian-like in the opposite direction together with oscillatory subunits which change the clusters of synchronized units they belong to. For future work it would be very interesting to search for dynamical phases as result of non-reciprocal interactions in models of limit-cycle oscillators such as Stuart-Landau or Fitz-Hugh Nagumo oscillators which are also relevant as models for brain dynamics. Otherwise there are many ways to implement non-reciprocity to formerly symmetric couplings, for example in multiplex networks [37, 38], in networks with designed two anti-phase clusters [39, 40], or networks leading to emergent anti-phase clusters such as in [41, 42], or in networks with geometric frustration which have been constructed such that a continuum of attractors was generated together with a (dynamically generated) Watanabe-Strogatz phenomenon of dimensional reduction [36, 43, 44].

Appendix A: Appendix: Stability analysis of two anti-phase clusters of arbitrary sizes

Consider the original fully connected Kuramoto model in the absence of noise ($\sigma_{\text{noise}} = 0$) with $\omega_i = 0 \forall i = 1, 2, 3, \dots, N$. Assume the oscillators form two anti-phase clusters, named Cluster A and Cluster B, of sizes

N_A and $N_B = N - N_A$, with phases

$$\theta_i = \begin{cases} \theta_A, & i \in \text{Cluster A}, \\ \theta_B = \theta_A + \pi, & i \in \text{Cluster B}. \end{cases} \quad (\text{A1})$$

The state vector is

$$\mathbf{x} = (\theta_1, \dots, \theta_N, k_{ij} \text{ for } i \neq j) \in \mathbb{R}^{N+N(N-1)}, \quad (\text{A2})$$

where we exclude the fixed diagonal elements $k_{ii} = 0$. Linearizing the dynamics around the two-cluster solution, the Jacobian takes the four-block form:

$$\mathbf{J} = \begin{pmatrix} \mathbf{J}_{\theta\theta} & \mathbf{J}_{\theta k} \\ \mathbf{J}_{k\theta} & \mathbf{J}_{kk} \end{pmatrix}. \quad (\text{A3})$$

with $\mathbf{J}_{\theta\theta}$: $N \times N$, phase–phase interactions; $\mathbf{J}_{\theta k}$: $N \times N(N-1)$, effect of couplings on phases; $\mathbf{J}_{k\theta}$: $N(N-1) \times N$, effect of phases on couplings; \mathbf{J}_{kk} : $N(N-1) \times N(N-1)$, coupling–coupling interactions.

Let us denote the blocks of the Jacobian as follows:

Phase–Phase block: $\mathbf{J}_{\theta\theta}$ The entries are

$$(\mathbf{J}_{\theta\theta})_{ij} = \frac{\partial \dot{\theta}_i}{\partial \theta_j} = \frac{\partial}{\partial \theta_j} \left[\omega_i + \frac{1}{N} \sum_{m=1}^N k_{im} \sin(\theta_m - \theta_i) \right]. \quad (\text{A4})$$

Evaluating the derivative gives

$$(\mathbf{J}_{\theta\theta})_{ij} = \begin{cases} -\frac{1}{N} \sum_{m \neq i} k_{im} \cos(\theta_m - \theta_i), & i = j, \\ \frac{1}{N} k_{ij} \cos(\theta_j - \theta_i), & i \neq j. \end{cases} \quad (\text{A5})$$

Phase–Coupling Block: $\mathbf{J}_{\theta k}$ This block captures how changes in couplings affect the phase dynamics:

$$(\mathbf{J}_{\theta k})_{i,(j \neq l)} = \frac{\partial \dot{\theta}_i}{\partial k_{jl}} = \begin{cases} \frac{1}{N} \sin(\theta_l - \theta_i), & j = i, \\ 0, & j \neq i. \end{cases} \quad (\text{A6})$$

Coupling–Phase Block: $\mathbf{J}_{k\theta}$ This block gives how the phases affect the evolution of couplings:

$$\begin{aligned} (\mathbf{J}_{k\theta})_{(i \neq j),m} &= \frac{\partial \dot{k}_{ij}}{\partial \theta_m} \\ &= \begin{cases} -\varepsilon_1 \cos(\theta_i - \theta_j - \pi/2), & i < j, m = i, \\ \varepsilon_1 \cos(\theta_i - \theta_j - \pi/2), & i < j, m = j, \\ -\varepsilon_2 \cos(\theta_i - \theta_j + \pi/2), & i > j, m = i, \\ \varepsilon_2 \cos(\theta_i - \theta_j + \pi/2), & i > j, m = j, \\ 0, & \text{otherwise.} \end{cases} \end{aligned} \quad (\text{A7})$$

Coupling–Coupling Block: \mathbf{J}_{kk} Finally, the effect of couplings on themselves is diagonal:

$$\begin{aligned} (\mathbf{J}_{kk})_{(i \neq j),(l \neq m)} &= \frac{\partial \dot{k}_{ij}}{\partial k_{lm}} \\ &= \begin{cases} -\varepsilon_1, & i < j \text{ and } (i, j) = (l, m), \\ -\varepsilon_2, & i > j \text{ and } (i, j) = (l, m), \\ 0, & \text{otherwise.} \end{cases} \end{aligned} \quad (\text{A8})$$

Phase–Coupling Block is Zero For the two-cluster configuration, each oscillator in cluster A has phase θ_A , and each in cluster B has $\theta_B = \theta_A + \pi$. Thus, for any entry of the phase–coupling block

$$(\mathbf{J}_{\theta k})_{i,(j \neq l)} = \frac{\partial \dot{\theta}_i}{\partial k_{jl}} = \begin{cases} \frac{1}{N} \sin(\theta_l - \theta_i), & j = i, \\ 0, & j \neq i, \end{cases}$$

we have two possibilities:

- If θ_l and θ_i belong to the same cluster, then $\theta_l - \theta_i = 0 \implies \sin(\theta_l - \theta_i) = 0$.
- If θ_l and θ_i belong to different clusters, then $\theta_l - \theta_i = \pm\pi \implies \sin(\theta_l - \theta_i) = 0$ as well.

Hence, for all i, j, l ,

$$(\mathbf{J}_{\theta k})_{i,(j \neq l)} = 0 \implies \mathbf{J}_{\theta k} = \mathbf{0}_{N \times N(N-1)}.$$

Eigenvalues via block-triangular structure For the two-cluster state, we have shown that the phase–coupling block vanishes:

$$\mathbf{J}_{\theta k} = \mathbf{0}_{N \times N(N-1)}.$$

Hence, the Jacobian becomes block lower-triangular:

$$\mathbf{J} = \begin{pmatrix} \mathbf{J}_{\theta\theta} & \mathbf{0} \\ \mathbf{J}_{k\theta} & \mathbf{J}_{kk} \end{pmatrix}.$$

Recall that the determinant of a block-triangular matrix is the product of the determinants of the diagonal blocks:

$$\det \begin{pmatrix} \mathbf{A} & \mathbf{0} \\ \mathbf{C} & \mathbf{B} \end{pmatrix} = \det(\mathbf{A}) \cdot \det(\mathbf{B}),$$

and applying this to \mathbf{J} gives the characteristic polynomial:

$$\det(\mathbf{J} - \lambda \mathbf{I}) = \det(\mathbf{J}_{\theta\theta} - \lambda \mathbf{I}_N) \cdot \det(\mathbf{J}_{kk} - \lambda \mathbf{I}_{N(N-1)}). \quad (\text{A9})$$

By definition, the eigenvalues are the roots of $\det(\mathbf{J} - \lambda \mathbf{I}) = 0$. From the above factorization, the eigenvalues of \mathbf{J} are exactly the eigenvalues of the two diagonal blocks:

$$\text{eig}(\mathbf{J}) = \text{eig}(\mathbf{J}_{\theta\theta}) \cup \text{eig}(\mathbf{J}_{kk}).$$

This proves that, due to the vanishing phase–coupling block, the spectrum of the full Jacobian splits into the spectra of $\mathbf{J}_{\theta\theta}$ and \mathbf{J}_{kk} .

Reduction to the Phase–Phase Block From the previous discussion, we have

$$\mathbf{J}_{kk} = \text{diag}(-\varepsilon_1, \dots, -\varepsilon_1, -\varepsilon_2, \dots, -\varepsilon_2),$$

where each diagonal entry is strictly negative. Therefore, all eigenvalues of \mathbf{J}_{kk} satisfy $\lambda(\mathbf{J}_{kk}) < 0$. Since the full Jacobian \mathbf{J} is block lower-triangular, $\text{eig}(\mathbf{J}) = \text{eig}(\mathbf{J}_{\theta\theta}) \cup \text{eig}(\mathbf{J}_{kk})$, any positive eigenvalue of \mathbf{J} can only arise from $\mathbf{J}_{\theta\theta}$. **Conclusion:** The stability of the two-cluster state is entirely determined by the $N \times N$

phase–phase block $\mathbf{J}_{\theta\theta}$. The $N(N-1) \times N(N-1)$ coupling–coupling block \mathbf{J}_{kk} cannot generate any instability because it is diagonal with strictly negative entries. Hence, the analysis reduces to checking the eigenvalues of $\mathbf{J}_{\theta\theta}$ only, greatly simplifying the stability problem.

Properties of the Phase–Phase Block $\mathbf{J}_{\theta\theta}$ The entries of $\mathbf{J}_{\theta\theta}$ are real:

$$(\mathbf{J}_{\theta\theta})_{ij} = \begin{cases} -\frac{1}{N} \sum_{m \neq i} k_{im} \cos(\theta_m - \theta_i), & i = j, \\ \frac{1}{N} k_{ij} \cos(\theta_j - \theta_i), & i \neq j. \end{cases}$$

Row sum and zero eigenvalue: Observe that for each row i , the sum of entries is

$$\begin{aligned} \sum_{j=1}^N (\mathbf{J}_{\theta\theta})_{ij} &= -\frac{1}{N} \sum_{m \neq i} k_{im} \cos(\theta_m - \theta_i) \\ &\quad + \sum_{j \neq i} \frac{1}{N} k_{ij} \cos(\theta_j - \theta_i) \\ &= 0. \end{aligned}$$

Therefore, $\mathbf{J}_{\theta\theta}$ always has one eigenvalue exactly equal to zero: $\lambda_0 = 0$. This zero eigenvalue corresponds to the rotational invariance of the Kuramoto model. Shifting all phases by a constant amount $\theta_i \mapsto \theta_i + \phi_0$ does not change the dynamics, so perturbations along this uniform phase shift direction neither grow nor decay. Hence, the zero eigenvalue represents a neutral mode associated with the global phase of the two-cluster solution.

Symmetry of eigenvalues. At the two-cluster anti-phase equilibrium, the couplings attain their asymptotic values:

$$k_{ij}^{\text{eq}} = \begin{cases} -\sin(\theta_i - \theta_j - \pi/2), & i < j, \\ -\sin(\theta_i - \theta_j + \pi/2), & i > j, \end{cases} \quad (\text{A10})$$

where $k_{ii}^{\text{eq}} = 0$. Using these equilibrium couplings, the entries of the phase–phase Jacobian become

$$(\mathbf{J}_{\theta\theta})_{ij} = \begin{cases} -\frac{1}{N} \sum_{m \neq i} k_{im}^{\text{eq}} \cos(\theta_m - \theta_i), & i = j, \\ \frac{1}{N} k_{ij}^{\text{eq}} \cos(\theta_j - \theta_i), & i \neq j, \end{cases} \quad (\text{A11})$$

and one can verify that the row sums vanish: $\sum_{j=1}^N (\mathbf{J}_{\theta\theta})_{ij} = 0, \forall i$. Hence, the Jacobian $\mathbf{J}_{\theta\theta}$ always has at least one zero eigenvalue, corresponding to the uniform phase shift mode: $\lambda_0 = 0$. All entries of $\mathbf{J}_{\theta\theta}$ are real. Let us define the exchange (or flip) matrix $\chi \in \mathbb{R}^{N \times N}$ as

$$\chi = \begin{pmatrix} 0 & 0 & \cdots & 0 & 1 \\ 0 & 0 & \cdots & 1 & 0 \\ \vdots & \vdots & \ddots & \vdots & \vdots \\ 0 & 1 & \cdots & 0 & 0 \\ 1 & 0 & \cdots & 0 & 0 \end{pmatrix}. \quad (\text{A12})$$

This matrix is self-inverse, $\chi^2 = I_N$, and it satisfies the relation $\chi \mathbf{J}_{\theta\theta} \chi = -\mathbf{J}_{\theta\theta}$. As a consequence, since $\chi \mathbf{J}_{\theta\theta} \chi = -\mathbf{J}_{\theta\theta}$ is a similarity transformation, the eigenvalues of $\mathbf{J}_{\theta\theta}$ occur in symmetric pairs: if λ is an eigenvalue, then $-\lambda$ is also an eigenvalue. This property is useful for analyzing the stability of the two-cluster solution.

Eigenvalue spectrum of $\mathbf{J}_{\theta\theta}$: The phase–phase block $\mathbf{J}_{\theta\theta}$ always has at least one zero eigenvalue corresponding to the uniform phase shift mode. Combining this with the eigenvalue symmetry under the exchange matrix χ , we can characterize the spectrum as follows:

- If $N = 2m + 1$ is odd, $\mathbf{J}_{\theta\theta}$ has one zero eigenvalue, m positive eigenvalues, and m negative eigenvalues. Moreover, the positive and negative eigenvalues have equal absolute values.
- If $N = 2m$ is even, $\mathbf{J}_{\theta\theta}$ has two zero eigenvalues, $m-1$ positive eigenvalues, and $m-1$ negative eigenvalues, again with matching absolute values.

Hence, as N increases, the number of positive eigenvalues grows, indicating an increasing number of unstable directions for the two-cluster solution.

Eigenvalues of $\mathbf{J}_{\theta\theta}$: By explicitly solving $\mathbf{J}_{\theta\theta}$ for the two-cluster configuration, one finds that the positive eigenvalues take the form

$$\lambda_k = 1 - \frac{2k}{N}, \quad k = 1, 2, \dots, n_+, \quad (\text{A13})$$

where n_+ is the number of positive eigenvalues. The corresponding negative eigenvalues are

$$\lambda_{-k} = -\lambda_k = -\left(1 - \frac{2k}{N}\right), \quad k = 1, 2, \dots, n_-, \quad (\text{A14})$$

with $n_+ = n_-$, reflecting the eigenvalue symmetry of $\mathbf{J}_{\theta\theta}$. Thus, for general N , the eigenvalues of $\mathbf{J}_{\theta\theta}$ consist of symmetric positive and negative pairs, along with one or two zero eigenvalues depending on whether N is odd or even. As N increases, the number of positive eigenvalues increases, indicating that the two-cluster configuration becomes less stable in larger networks.

Numerical Validation: To investigate the local stability of the two anti-phase clusters, we analyze the phase–phase block of the Jacobian, $J_{\theta\theta}$ (given in Eq. (A11)), corresponding to a given bipartition of N oscillators. For each bipartition, we construct the equilibrium phases $\theta_i = 0$ for one cluster and $\theta_i = \pi$ for the other, and compute the real parts of the eigenvalues of $J_{\theta\theta}$. Due to the large number of possible bipartitions, a full enumeration is computationally infeasible. Indeed, the total number of distinct bipartitions for a system of N oscillators is

$$\frac{1}{2} \sum_{k=1}^{N-1} \binom{N}{k} = 2^{N-1} - 1,$$

which for $N = 20$ amounts to 524,287 possible configurations. Therefore, we adopt a random sampling strategy,

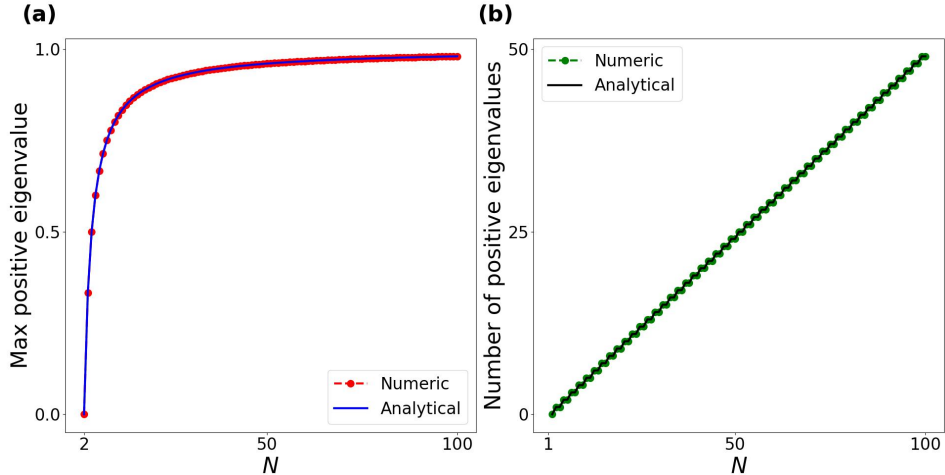


FIG. 14. Stability analysis of the two-cluster anti-phase state using the phase-phase block J_{00} (given in Eq. (A11)) of the Jacobian. (a) Maximum positive eigenvalue as a function of N . (b) Maximum number of positive eigenvalues as a function of the number of oscillators N . The results confirm that the numerical maxima agree with the analytical predictions.

selecting 500 random bipartitions for each N . This approach allows us to efficiently approximate the maximal number of positive eigenvalues and the largest positive eigenvalue while keeping the computational cost reasonable. The results of this procedure are summarized in Fig. (14), which shows the maximal positive eigenvalue and the number of positive eigenvalues as functions of N . Clearly, as N increases, both the number of positive eigenvalues and the maximum positive eigenvalue grow, with the latter approaching the theoretical limit of 1.

CONFLICT OF INTEREST STATEMENT

The authors declare that the research was conducted in the absence of any commercial or financial relationships that could be construed as a potential conflict of interest.

AUTHOR CONTRIBUTIONS

The project was conceived by H.M.-O. The simulations and analytical calculations were performed by S.N.C. Both authors contributed to a first draft of the manuscript. H.M.-O. is responsible for the final version.

Both authors agree about the final version.

FUNDING

Financial support by the Deutsche Forschungsgemeinschaft (DFG) through Grant No. ME-1332/30-1 is gratefully acknowledged. Furthermore, the simulations were performed on a computer cluster funded through the project INST 676/7-1 FUGG.

ACKNOWLEDGMENTS

We would like to thank Dr. Tuan Minh Pham (University of Amsterdam) for stimulating discussions.

DATA AVAILABILITY STATEMENT

The original contributions presented in the study are included in the article/Supplementary Material. Further inquiries can be directed to the corresponding author.

[1] Haim Sompolinsky and Ido Kanter. Temporal association in asymmetric neural networks. *Physical Review Letters*, 57(22):2861, 1986.

[2] Philip Seliger, Stephen C Young, and Lev S Tsimring. Plasticity and learning in a network of coupled phase oscillators. *Physical Review E*, 65:041906, 2002.

[3] David Papo and Javier M Buldú. Biological detail and graph structure in network neuroscience. *Frontiers in Network Physiology*, 5:1667656, 2025.

[4] Ricardo Gutiérrez, Andreas Amann, Salvatore Assenza, Jesús Gómez-Gardenes, V Latora, and Stefano Boccaletti. Emerging meso-and macroscales from synchronization of adaptive networks. *Physical Review Letters*, 107(23):234103, 2011.

[5] Xiyun Zhang, Stefano Boccaletti, Shuguang Guan, and Zonghua Liu. Explosive synchronization in adaptive

and multilayer networks. *Physical Review Letters*, 114(3):038701, 2015.

[6] Rico Berner, Jakub Sawicki, and Eckehard Schöll. Birth and stabilization of phase clusters by multiplexing of adaptive networks. *Physical Review Letters*, 124(8):088301, 2020.

[7] Jakub Sawicki, Rico Berner, Thomas Löser, and Eckehard Schöll. Modeling tumor disease and sepsis by networks of adaptively coupled phase oscillators. *Frontiers in Network Physiology*, 1:730385, 2022.

[8] Marzena Ciszak, Francesco Marino, Alessandro Torcini, and Simona Olmi. Emergent excitability in populations of nonexcitable units. *Physical Review E*, 102(5):050201, 2020.

[9] Rico Berner, Serhiy Yanchuk, and Eckehard Schöll. What adaptive neuronal networks teach us about power grids. *Physical Review E*, 103(4):042315, 2021.

[10] Rico Berner, Serhiy Yanchuk, and Eckehard Schöll. Modelling power grids as pseudo adaptive networks. *arXiv preprint arXiv:2104.06128*, 2021.

[11] DV Kasatkin, S Yanchuk, E Schöll, and VI Nekorkin. Self-organized emergence of multilayer structure and chimera states in dynamical networks with adaptive couplings. *Physical Review E*, 96(6):062211, 2017.

[12] Dmitry V Kasatkin and Vladimir I Nekorkin. The effect of topology on organization of synchronous behavior in dynamical networks with adaptive couplings. *The European Physical Journal Special Topics*, 227(10):1051–1061, 2018.

[13] Takaaki Aoki. Self-organization of a recurrent network under ongoing synaptic plasticity. *Neural Networks*, 62:11–19, 2015.

[14] Oleksandr V Popovych, Serhiy Yanchuk, and Peter A Tass. Self-organized noise resistance of oscillatory neural networks with spike timing-dependent plasticity. *Scientific Reports*, 3(1):2926, 2013.

[15] Hyunsuk Hong and Steven H Strogatz. Kuramoto model of coupled oscillators with positive and negative coupling parameters: an example of conformist and contrarian oscillators. *Physical Review Letters*, 106(5):054102, 2011.

[16] François A Lavergne, Hugo Wendehenne, Tobias Bäuerle, and Clemens Bechinger. Group formation and cohesion of active particles with visual perception-dependent motility. *Science*, 364(6435):70–74, 2019.

[17] Nariya Uchida and Ramin Golestanian. Synchronization and collective dynamics in a carpet of microfluidic rotors. *Physical Review Letters*, 104(17):178103, 2010.

[18] Máté Nagy, Zsuzsa Ákos, Dora Biro, and Tamás Vicsek. Hierarchical group dynamics in pigeon flocks. *Nature*, 464(7290):890–893, 2010.

[19] Martin Brandenbourger, Xander Locsin, Edan Lerner, and Corentin Coulais. Non-reciprocal robotic metamaterials. *Nature Communications*, 10(1):4608, 2019.

[20] Mohammad-Ali Miri and Andrea Alu. Exceptional points in optics and photonics. *Science*, 363(6422):eaar7709, 2019.

[21] Sayantan Nag Chowdhury, Srileena Kundu, Maja Duh, Matjaž Perc, and Dibakar Ghosh. Cooperation on interdependent networks by means of migration and stochastic imitation. *Entropy*, 22(4):485, 2020.

[22] Ernest Montbrió and Diego Pazó. Kuramoto model for excitation-inhibition-based oscillations. *Physical Review Letters*, 120(24):244101, 2018.

[23] Michel Fruchart, Ryo Hanai, Peter B Littlewood, and Vincenzo Vitelli. Non-reciprocal phase transitions. *Nature*, 592(7854):363–369, 2021.

[24] Emmanuelle Tognoli and JA Scott Kelso. The metastable brain. *Neuron*, 81(1):35–48, 2014.

[25] Misha Rabinovich, Ramon Huerta, and Gilles Laurent. Transient dynamics for neural processing. *Science*, 321(5885):48–50, 2008.

[26] Mikhail I Rabinovich and Pablo Varona. Robust transient dynamics and brain functions. *Frontiers in Computational Neuroscience*, 5:24, 2011.

[27] JA Scott Kelso. *Dynamic patterns: The self-organization of brain and behavior*. MIT press, 1995.

[28] Karl J Friston. Transients, metastability, and neuronal dynamics. *Neuroimage*, 5(2):164–171, 1997.

[29] Hildegard Meyer-Ortmanns. Heteroclinic networks for brain dynamics. *Frontiers in Network Physiology*, 3:1276401, 2023.

[30] Karel L Rossi, Roberto C Budzinski, Everton S Medeiros, Bruno RR Boaretto, Lyle Muller, and Ulrike Feudel. Dynamical properties and mechanisms of metastability: A perspective in neuroscience. *Physical Review E*, 111(2):021001, 2025.

[31] Rico Berner, Thilo Gross, Christian Kuehn, Jürgen Kurths, and Serhiy Yanchuk. Adaptive dynamical networks. *Physics Reports*, 1031:1–59, 2023.

[32] Zhen Wang, Sara Baruni, Fatemeh Parastesh, Sajad Jafari, Dibakar Ghosh, Matjaž Perc, and Iqtadar Hussain. Chimeras in an adaptive neuronal network with burst-timing-dependent plasticity. *Neurocomputing*, 406:117–126, 2020.

[33] Frank Harary. A matrix criterion for structural balance. *Naval Research Logistics Quarterly*, 7(2):195–199, 1960.

[34] Sayantan Nag Chowdhury. Metastability in kuramoto oscillators. <https://github.com/SayantanNagChowdhury/Metastability-in-Kuramoto-Oscillators>, 2025. Accessed: 2025-11-26.

[35] Mark S Granovetter. The strength of weak ties. *American Journal of Sociology*, 78(6):1360–1380, 1973.

[36] Darka Labavić and Hildegard Meyer-Ortmanns. Long-period clocks from short-period oscillators. *Chaos: An Interdisciplinary Journal of Nonlinear Science*, 27(8), 2017.

[37] Sayantan Nag Chowdhury, Sarbendu Rakshit, Chittaranjan Hens, and Dibakar Ghosh. Interlayer antisynchronization in degree-biased duplex networks. *Physical Review E*, 107(3):034313, 2023.

[38] Sayantan Nag Chowdhury, Sarbendu Rakshit, Javier M Buldu, Dibakar Ghosh, and Chittaranjan Hens. Antiphase synchronization in multiplex networks with attractive and repulsive interactions. *Physical Review E*, 103(3):032310, 2021.

[39] Sayantan Nag Chowdhury, Md Sayeed Anwar, and Dibakar Ghosh. Cluster formation due to repulsive spanning trees in attractively coupled networks. *Physical Review E*, 109(4):044314, 2024.

[40] Sayantan Nag Chowdhury, Dibakar Ghosh, and Chittaranjan Hens. Effect of repulsive links on frustration in attractively coupled networks. *Physical Review E*, 101(2):022310, 2020.

[41] Sayantan Nag Chowdhury, Soumen Majhi, and Dibakar Ghosh. Distance dependent competitive interactions in a frustrated network of mobile agents. *IEEE Transactions on Network Science and Engineering*, 7(4):3159–

3170, 2020.

[42] Gourab K Sar, Sayantan Nag Chowdhury, Matjaž Perc, and Dibakar Ghosh. Swarmalators under competitive time-varying phase interactions. *New Journal of Physics*, 24(4):043004, 2022.

[43] Florin Ionita, Darka Labavić, Michael A Zaks, and Hildegard Meyer-Ortmanns. Order-by-disorder in classical oscillator systems. *The European Physical Journal B*, 86(12):511, 2013.

[44] Darka Labavić and Hildegard Meyer-Ortmanns. Temporal self-similar synchronization patterns and scaling in repulsively coupled oscillators. In *Indian Academy of Sciences Conference Series*, volume 1, page 101, 2017.